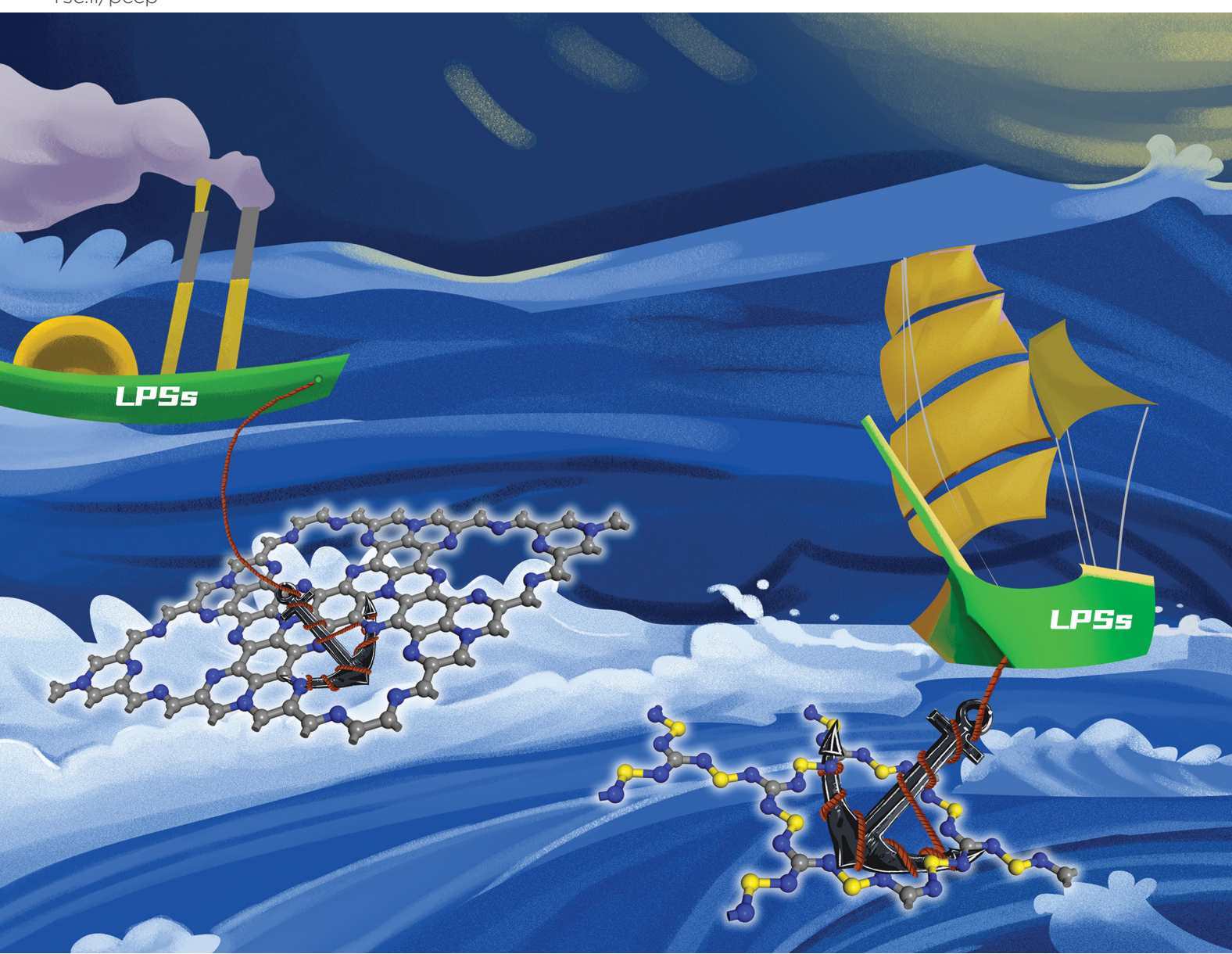
Volume 23 Number 23 21 June 2021 Pages 12911-13420

PCCP

Physical Chemistry Chemical Physics

rsc.li/pccp



ISSN 1463-9076



PAPER

Fengyu Li, Jian Gong, Zhongfang Chen et al. C_9N_4 and $C_2N_6S_3$ monolayers as promising anchoring materials for lithium–sulfur batteries: weakening the shuttle effect \emph{via} optimizing lithium bonds

PCCP



View Article Online **PAPER**



Cite this: Phys. Chem. Chem. Phys., 2021, 23, 12958

C₉N₄ and C₂N₆S₃ monolayers as promising anchoring materials for lithium-sulfur batteries: weakening the shuttle effect via optimizing lithium bonds†

Yinan Dong,^a Bai Xu,^a Haiyu Hu,^a Jiashu Yang,^a Fengyu Li, ^b* Jian Gong* and Zhongfang Chen *b

The notorious polysulfide shuttle effect is a crucial factor responsible for the degradation of Li-S batteries. A good way to suppress the shuttle effect is to effectively anchor dissoluble lithium polysulfides (LPSs, Li_2S_n) on appropriate substrates. Previous studies have revealed that Li of Li_2S_n is prone to interact with the N of N-containing materials to form Li-N bonds. In this work, by means of density functional theory (DFT) computations, we explored the possibility to form Li bonds on ten different N-containing monolayers, including BN, C₂N, C₂N₆S₃, C₉N₄, a covalent triazine framework (CTF), $g-C_3N_4$, $p-C_3N_4$, C_3N_5 , $S-N_2S$, and $T-N_2S$, by examining the adsorption behavior of Li_2S_n (n=1,2, 3, 4, 6, 8) on these two-dimensional (2D) anchoring materials (AMs), and investigated the performance of the formed Li bonds (if any) in inhibiting the shuttle effect. By comparing and analyzing the nitrogen content, the N-containing pore size, charge transfer, and Li bonds, we found that the N content and N-containing pore size correlate with the number of Li bonds, and the formed Li-N bonds between LPSs and AMs correspond well with the adsorption energies of the LPSs. The C_9N_4 and $C_7N_6S_7$ monolayers were identified as promising AMs in Li-S batteries. From the view of Li bonds, this work provides guidelines for designing 2D N-containing materials as anchoring materials to reduce the shuttle effect in Li-S batteries, and thus improving the performance of Li-S batteries.

Received 8th March 2021, Accepted 5th May 2021

DOI: 10.1039/d1cp01022k

rsc.li/pccp

1. Introduction

The increasing energy demand, accelerating global climate change, and worsening environment all are calling for the replacement of traditional fossil fuel energy by renewable energies. Lithiumsulfur (Li-S) batteries have a rather high theoretical specific capacity

 $(1675 \text{ mA h g}^{-1})$ and a high energy density $(2600 \text{ W h kg}^{-1})$, as well as a low application cost and abundant natural reserves, and thus are among the most promising renewable energies, especially as the next generation energy storage devices for electric vehicles.²⁻⁴ However, the development of Li-S batteries has suffered many obstacles, such as low S utilization, poor cycle life, and volume expansion.⁵⁻⁹ The polysulfide "shuttle effect", which originates from the migration of the electrically insulating sulfur and the dissoluble lithium polysulfides (LPSs, Li_2S_n) between the anode and cathode during charging and discharging processes, is one of the most important unsolved issues that limit the practical application of Li-S batteries.

A good strategy to suppress the shuttle effect is to introduce polar functional groups 10 or anchoring materials (AMs) to strongly bind the Li_2S_n species, thus reducing the leakage of active material from the cathode. 11 For example, vacancy defects and heteroatomdoping can improve the adsorption capability of graphene nanoribbons (GNRs), 12,13 graphene, 14,15 and BN. 16 Two-dimensional (2D) carbon-based N-containing materials, such as C₂N¹⁷ and g-C₃N₄, ¹⁸⁻²³ demonstrate their good performance as AMs. Note that the interaction between the LPSs and the AM should be moderate, otherwise it will result in irreversible dissociation of

^a School of Physical Science and Technology, Inner Mongolia University, Hohhot, 010021, China. E-mail: fengyuli@imu.edu.cn, ndgong@imu.edu.cn

^b Department of Chemistry, The Institute for Functional Nanomaterials, University of Puerto Rico, Rio Piedras Campus, San Juan, PR. 00931, USA. E-mail: zhongfangchen@gmail.com

[†] Electronic supplementary information (ESI) available: The most stable configurations of Li₂S_n and S₈ on the AMs; top and side views of the "intact" and decomposed Li₂S₄ on the C₉N₄ and C₂N₆S₃, as well as their relative energies; diffusion paths and migration energy barriers of Li₂S₆ on the BN, C₉N₄, C₂N₆S₃ and CTF monolayers; charge density difference diagrams and the most stable configurations of Li₂S_n and S₈ on different AMs; linear fitting between the adsorption energy of Li_2S_n (n = 1-4, 6, 8) and the pore size of the AMs; average length of S–C bond ($d_{\text{S-C}}$) and S–N bond ($d_{\text{S-N}}$) for different AMs; Li···S distances of the broken Li–S bonds ($d_{\text{Li}\cdots\text{S}}$, in Å). Data in parentheses denote the number of broken Li-S bonds; average length of the formed S-N bond (d_{S-N}) between the Li_2S_n and the ten AMs; variation of adsorption energies (E_{ad}) , charge transfer (Δq) and average length of Li-S/N bond ($d_{\text{Li-S}}$, $d_{\text{Li-N}}$). See DOI: 10.1039/d1cp01022k

Paper

the lithium polysulfides. For example, the excessive strength of the Li-O/Li-S bonds between Li₂S_n and metal oxides/metal sulfides leads to Li_2S_n dissociation, thus weakening the adsorption effect for such metal oxides and metal sulfides. 11,24,25

Very recently, the importance of Li bonds^{26,27} in Li-S batteries has gained attention in the battery community. In 2015, for the first time, Goodenough and coworkers reported spectroscopic evidence of the existence of Li bonds between LPSs and the polymer matrix, which resist the dissolution of LPSs and thus ease the shuttle effect in Li-S batteries.²⁸ Shortly afterwards, Zhang and coworkers performed very detailed theoretical and experimental studies from the aspects of the chemical bonds, and provided solid proof of Li bonds in Li-S batteries.²⁹ Ever since, Li bond theory has been widely used to explain the nature and behavior of LPSs-AM interactions, and to gain insights into the fundamental Li chemistry in batteries.³⁰

Considering the importance of Li bonds in inhibiting lithium polysulfides shuttling, some interesting questions are naturally raised: what physicochemical features of the AMs are affecting the strength of the Li bonds? Is there any correlation? Answering these questions can provide us with some guidelines in designing cathode materials for Li-S batteries.

To address the above mentioned questions, in this work, we performed systematic density functional theory (DFT) computations to investigate the adsorption behavior of LPSs and S₈ adsorbed on ten different N-containing 2D materials, namely, C₉N₄,³¹ C₂N,³² BN,³³ a covalent triazine framework (CTF),³⁴ $C_2N_6S_3$, 35 g- C_3N_4 , $^{36-38}$ p- C_3N_4 , 39 C_3N_5 , 40,41 S- N_2S , 42 and T- N_2S . 43 These candidate anchoring materials are either experimentally available, or have been theoretically identified as experimentally feasible materials. Among them, C₂N₆S₃ and C₉N₄ feature Dirac cones, and their good electrical conductivity is rather beneficial for battery electrode materials. It is known that the overall reaction equation of the discharge process in the Li-S battery is $S_8 + 16Li \rightarrow 8Li_2S$, which involves multiple steps and Li_2S_n as a product in each step. ⁴⁴ Herein, we chose Li_2S_n (n = 1, 2, 3, 4, 6, 8) to study the adsorption behavior of LPSs on the ten considered AMs. By comparing and analyzing the stable configuration, adsorption energies, and charge transfer, we found that the N-containing pore size, the chemical environment of the N atoms, and the amount of charge transfer contribute to the adsorption strength of Li₂S_n. Our computations identified C₉N₄ and C₂N₆S₃ monolayers as promising anchoring materials, and highlighted the importance of Li bonds when designing cathode materials for Li-S batteries.

2. Computation methods

Spin-polarized density functional theory (DFT) calculations were carried out using the Vienna ab initio simulation package (VASP). 45-50 The projector augmented wave (PAW) method 51 was used to describe the electron-ion interactions, and the Perdew-Burke-Ernzerhof (PBE)⁵² functional with the Generalized Gradient Approximations (GGA) was adopted for electron-electron exchange correlations. The energy cutoff and k-point mesh were

set to be 500 eV and 5 \times 5 \times 1, respectively. The geometric structures were optimized with the convergence criteria of the total energy less than 10⁻⁵ eV and total force less than 0.01 eV Å^{-1} on each atom. A supercell consisting of 5 \times 5 \times 1 (BN, S-N₂S, T-N₂S) or $2 \times 2 \times 1$ (C₉N₄, C₂N, CTF, C₂N₆S₃, g-C₃N₄, p-C₃N₄, C₃N₅) unit cells with the lateral dimensions of 12.56-30.28 Å was adopted. A vacuum region of about 25 Å was applied to the z-direction. Previous studies have shown that the van der Waals (vdW) interaction significantly affects the stable adsorption configuration and adsorption energy of Li_2S_n on AMs. ^{11,53} Therefore, the D2 method⁵⁴ is adopted to describe the interaction between Li₂S_n adsorption and AMs to obtain more accurate calculation results. The Bader charge analysis 55-57 was used to evaluate the charge transfer between the LPSs and AMs. The migration energy barrier of Li_2S_n on these 2D materials was determined using the climbing image nudged elastic-band (CI-NEB) method.58

Note that the solvent effect is very important in characterizing the performance of Li-S batteries, 53 and in our work, the solvent effect might relate to the detection ability of the N-containing monolayers. Considering the general impact of Li bonds on the shuttle effect, and to save the computation cost, the solvent effect was not involved here.

Fig. 1 presents the geometric structures of the examined AMs, Li_2S_n and S_8 ; Table S1 (ESI†) lists the N content (η), pore size (d), and the number of bridge N atoms (m) of each AM, where the η , d and x are defined as the percentage of N atoms, the distance between the two farthest N atoms in the same pore region, and the number of two-coordinated N atoms in one pore region, respectively. The adsorption energy (E_{ad}) of the Li_2S_n on the AMs in our work is defined as follows:

$$E_{\rm ad} = E_{\rm AM} + E_{\rm Li_2S_n} - E_{\rm tot} \tag{1}$$

where the E_{tot} , E_{AM} and $E_{\text{Li}_2S_n}$ are the total energy of Li_2S_n adsorbed on the AM, and the energies of pristine AM and isolated Li₂S_n, respectively. According to this definition, a more positive E_{ad} value indicates a stronger binding strength between the AM and the adsorbate.

Results and discussion

3.1. Adsorption of Li_2S_n on 2D AMs

First, we examined the adsorption of Li_2S_n at different sites on each AM, and identified the most stable configurations and calculated the corresponding adsorption energies (E_{ad}) , as given in Fig. S1 (ESI†), Fig. 2, 3, and Table 1. For Li_2S_n (n = 1, 2, 3, 4, 6, 8) and S₈ (Fig. 2), the BN monolayer has the lowest adsorption energies (0.52-1.28 eV), while the CTF shows the highest adsorption strength ($E_{\rm ad}$ = 1.25-6.45 eV). With the increase of n in Li_2S_n , the adsorption energy generally decreases on all examined AMs: the adsorption energy decreases from Li₂S to the lowest value at Li₂S₆, and then increases slightly for Li₂S₈ (Fig. 2 and Table 1). A similar trend was found for the adsorption of Li₂S_n on the transition metal oxides/sulfides/ chlorides25 and phosphorene.59

PCCP Paper

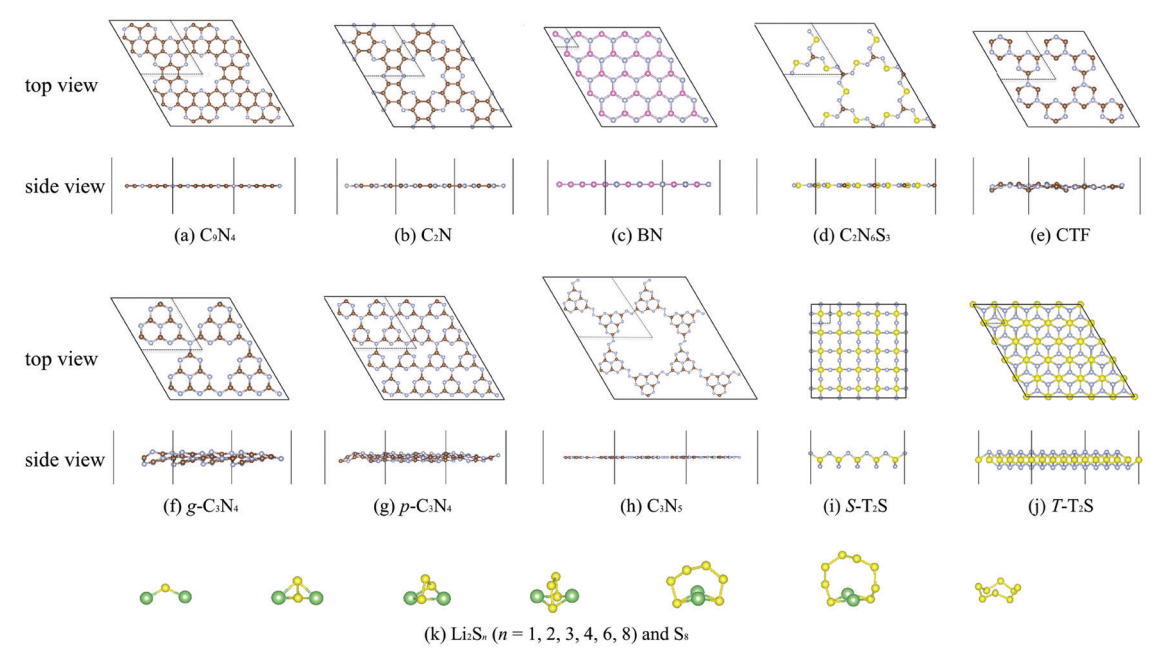


Fig. 1 Structures of 2D AMs (a–j), as well as Li_2S_n and S_8 (k). The black dashed area represents the unit cell. The pink, brown, gray, yellow, and green balls denote boron, carbon, nitrogen, sulfur, and lithium atoms, respectively.

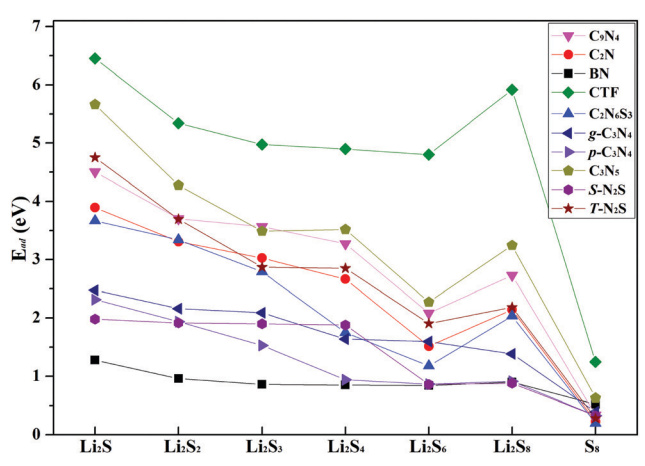


Fig. 2 Adsorption energies of Li_2S_n and S_8 on different AMs.

Then, we carefully analyzed the most stable adsorption configurations of Li_2S_n (n = 1, 2, 3, 4, 6, 8) and S_8 on all the examined 2D AMs. For clarity, in the main text, we only presented the energetically most favorable adsorption configurations of Li₂S_n and S₈ on BN and CTF (Fig. 3), while the data for other AMs are given in Fig. S1 (ESI†). Note that the BN and CTF monolayers have the lowest and highest adsorption energies towards LPSs among these ten AMs, and thus serve as good representatives.

For all these ten N-containing AMs, Li-N bonds are formed between the Li_2S_n and the AMs upon Li_2S_n adsorption. On one hand, Li₂S_n@BN has the longest Li-N bond lengths, and only one or two Li-N bonds are formed between Li_2S_n and the host, which explains well the lowest LPSs adsorption energies on BN among the examined AMs. Note that such small adsorption energies (0.90-1.28 eV) cannot prevent the migration of Li₂S_n,

and thus the BN monolayer cannot effectively inhibit the shuttle effect. On the other hand, in the case of Li_2S_n (a) CTF, which has the largest binding energies towards Li₂S_n, besides Li-N bonds, S-C bonds are also formed between the Li_2S_n and the CTF monolayer. Interestingly, with increasing the S content (n) of Li₂S_n, the number of the S-C bonds also increases (Table S2, ESI†), indicating the enhanced adsorption strength between Li_2S_n and the CTF host; however, at the same time, the average Li–S bond length of $\text{Li}_2S_n(d_{\text{Li-S}})$ increases with the increasing number of S atoms in the Li_2S_n species (Table 2), suggesting the higher tendency for dissociation of the Li_2S_n species. Therefore, as observed in the case of the CTF, very high Li_2S_n adsorption energies can lead to the dissociation of Li_2S_n species. The above analyses revealed that both BN and CTF monolayers are not good AMs for Li-S batteries, and a medium adsorption energy is significant to inhibit the shuttle effect. Such an adsorption should not be too weak in order to prevent the migration of LPSs, and also should not be too strong so that the dissociation of LPSs can be avoided.

The general trend between the Li_2S_n -AM interaction strength and the Li-S bond length of Li_2S_n observed for the two extreme cases (BN and CTF) holds true for all the AMs examined in this study. Due to the electrostatic interaction between the Li_2S_n and the AMs, the Li-N (S-N or S-S) bonds are formed, and simultaneously the Li-S bonds are stretched (by 0.02-0.39 Å) or even broken (Table S3, ESI†). The average Li-S bond length and the number of the broken Li-S bonds of the Li₂S_n adsorbed on the ten examined N-containing AMs are presented in Table 2 and Table S3 (ESI†).

Carefully examining the data in Tables 1 and 2 indicates that, besides BN and CTF, four of the other monolayers, namely, p-C₃N₄, S-N₂S, C₃N₅, and T-N₂S, can also be ruled out

PCCP Paper

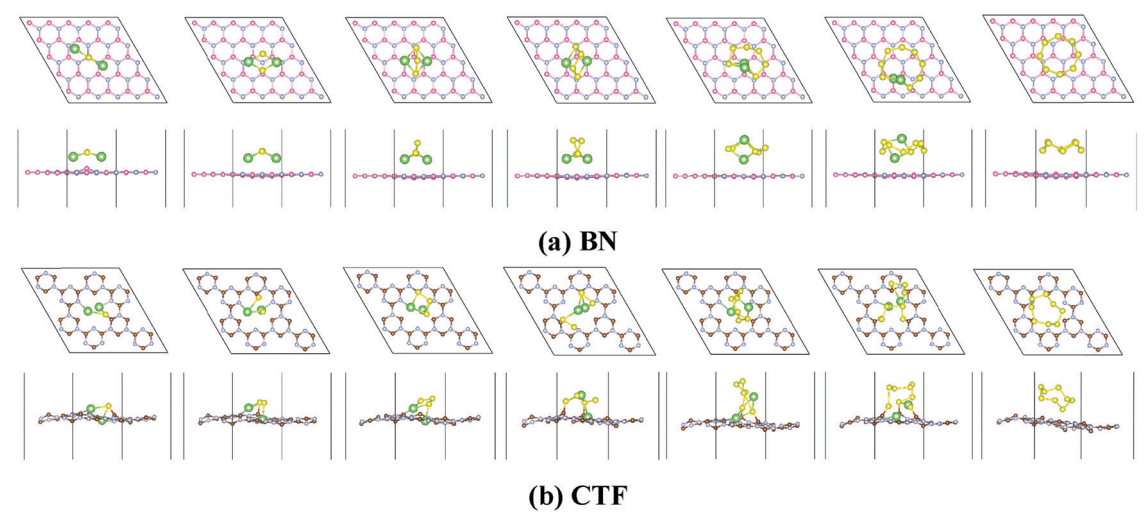


Fig. 3 The most stable adsorption configurations of Li_2S_n and S_8 on the BN (a) and CTF (b) monolayers. Color scheme: B, pink; N, blue; C, brown; Li, green; S, yellow.

as AMs for Li-S batteries. On p-C₃N₄ and S-N₂S, the adsorbed Li_2S_n species have similar and intact configurations; however, due to the rather weak adsorption strengths of Li2S6 and Li2S8 (0.86 and 0.91 eV, respectively, on p-C₃N₄; 0.86 and 0.88 eV, respectively, on S-N2S), the adsorbed Li2Sn may migrate on these two monolayers. On C₃N₅, the adsorbed Li₂S₃ and Li₂S₄, Li₂S₆, and Li₂S₈ all suffer Li-S bond breaking (the Li···S separations range from 2.97 to 4.62 Å). On T-N₂S, except for Li₂S₃ and Li₂S₄, Li-S bond breakage occurs for the other four adsorbed Li_2S_n (the $\text{Li} \cdot \cdot \cdot S$ distances are in the range of 2.96-4.00 Å, Table S3, ESI†); in particular, one S atom dissociates from the Li₂S₂ on the T-N₂S surface (Fig. S1, ESI†). The dissociation tendency of the adsorbed Li_2S_n suggests that C_3N_5 and T-N₂S monolayers are inappropriate AMs for Li-S batteries.

Encouragingly, among the AMs examined in this work, C₂N $(E_{ad} = 1.52-3.89 \text{ eV}), g-C_3N_4 (E_{ad} = 1.38-2.47 \text{ eV}), C_9N_4 (E_{ad} = 1.88-2.47 \text{ eV})$ 2.08-4.50 eV), and $C_2N_6S_3$ ($E_{ad} = 1.18-3.68$ eV) maintain a balance between the integrity of Li_2S_n and a strong adsorption strength. For the C₂N and g-C₃N₄ monolayers, our computational results, including the adsorption energies and structural variations of the Li₂S_n adsorption on these monolayers and the general conclusion that both C2N and g-C3N4 are good AMs for Li-S batteries, agree well with the previous studies. 17,18 Thus, we will only focus on the other two promising AMs, namely, C₉N₄ and C₂N₆S₃, in the following sections. Both C₉N₄ and C₂N₆S₃ have medium adsorption energies for LPSs, and the E_{ad} values for specific Li₂S_n species are very close to those on C₂N, which has been proven to be a promising AM for Li-S batteries.¹⁷

Both C_9N_4 and $C_2N_6S_3$ monolayers can adsorb Li_2S_n species without breaking the integrity of Li-S clusters. It is known that the long-chain Li_2S_n species (n = 4, 6, 8) tend to dissociate into smaller clusters.²² However, the adsorption of Li₂S₄, Li₂S₆, and even Li₂S₈ (the longest-chain Li₂S_n) on C₉N₄ or C₂N₆S₃ monolayers does not break any Li-S bonds (Table 2 and Table S3, ESI†). Upon the adsorption of short-chain Li_2S_n species (n = 1, 2, 3), the integrity of the Li₂S_n on both C₉N₄ and C₂N₆S₃

monolayers is well maintained. Interestingly, on the C₂N₆S₃ monolayer, in addition to the newly formed Li-N bonds, one S-S bond is formed between each Li₂S_n and the C₂N₆S₃ monolayer (the S-S bond length is 2.04, 2.48 and 2.49 Å for n = 1, 2and 3, respectively), and no Li-S bond is broken (except for the adsorption of Li₂S₃, and one Li-S bond is stretched to 3.68 Å).

In order to investigate whether LPSs can easily dissociate or not on C₉N₄ and C₂N₆S₃, we calculated the relative energies of "intact" and "decomposed" Li2S4 on the surface of C9N4 and C₂N₆S₃ (Fig. S2, ESI†). The "decomposed" Li₂S₄ on C₉N₄ and $C_2N_6S_3$ has a higher energy (0.83 and 1.24 eV, respectively) than its "intact" counterpart, indicating that the system of "intact" Li_2S_4 on either the C_9N_4 or $\text{C}_2\text{N}_6\text{S}_3$ monolayer is energetically more favorable. In other words, LPSs are energetically reluctant to dissociate on C₉N₄ and C₂N₆S₃ monolayers.

Good conductivity is an essential requirement of an AM for Li-S batteries, thus we investigated the electronic properties of C₉N₄ and C₂N₆S₃ before and after the adsorption of the LPSs. According to the density of states (DOS) of two AMs before and after the adsorption of LPSs (Fig. S3, ESI†), one can see that both AMs retain the metallic feature after the adsorption of the LPSs, and dominate the contribution of the total DOS (TDOS). Therefore, both C₉N₄ and C₂N₆S₃ have excellent electrical conductivity during the whole process of electrode reaction, which will significantly improve the performance of Li-S batteries.

3.2. Migration of Li₂S₆ on C₉N₄ and C₂N₆S₃ monolayers

To give a standard of "weak" and "suitable" adsorption energy, we calculated the migration energy barrier of the LPSs on the AMs, and Li₂S₆ was taken as the representative on BN, C₉N₄, C₂N₆S₃ and CTF, where BN/CTF has small/large adsorption energy, C₉N₄ and C₂N₆S₃ have medium adsorption energy. Among the three considered migration paths of Li₂S₆ on these AMs (Fig. S4, ESI†), path 2 has the lowest barriers (Table S5, ESI†), and the migration energy barriers were calculated to be 0.18, 0.81, 0.44 and 2.01 eV (Fig. S5, ESI†), respectively, on BN,

PCCP

Table 1 Adsorption energy (E_{ad}), the average length of the Li-N bond (d_{Li-N}) , and the amount of charge transfer (Δq) of Li_2S_n and S_8 on different AMs. Data in parentheses denote the number of Li-N bonds

	•						
	Li_2S	${\rm Li}_2{\rm S}_2$	$\mathrm{Li}_2\mathrm{S}_3$	$\mathrm{Li}_2\mathrm{S}_4$	Li_2S_6	$\mathrm{Li}_2\mathrm{S}_8$	S_8
$E_{\rm ad}/{\rm eV}$							
C_9N_4	4.50	3.70	3.57	3.28	2.08	2.73	0.33
C_2N	3.89	3.31	3.03	2.66	1.52	2.14	0.22
BN	1.28	0.96	0.86	0.85	0.84	0.90	0.52
CTF	6.45	5.34	4.98	4.90	4.80	5.92	1.25
$C_2N_6S_3$	3.68	3.34	2.79	1.75	1.18	2.03	0.20
g - C_3N_4	2.47	2.16	2.09	1.64	1.60	1.38	0.39
p-C ₃ N ₄	2.32	1.94	1.53	1.25	0.86	0.91	0.33
C_3N_5	5.66	4.28	3.60	3.52	2.27	3.24	0.63
S - N_2S	1.98	1.92	1.90	1.88	0.86	0.88	0.33
T - N_2S	4.75	3.70	2.87	2.85	1.90	2.18	0.28
$d_{\mathrm{Li-N}}/\mathrm{\mathring{A}}$							
C_9N_4	1.93	1.95	2.02	2.02	2.15	2.03	_
	(4)	(4)	(4)	(4)	(4)	(4)	_
C_2N	1.95	2.04	2.09	2.00	2.17	2.07	_
	(4)	(4)	(4)	(4)	(4)	(4)	
BN	2.10	2.22	2.26	2.26	2.22	2.14	_
	(2)	(2)	(2)	(2)	(1)	(1)	
CTF	1.99	2.00	1.99	2.06	2.21	2.04	_
	(2)	(2)	(2)	(1)	(1)	(1)	_
$C_2N_6S_3$	2.03	2.04	2.07	2.08	2.13	2.08	_
	(4)	(4)	(4)	(4)	(2)	(4)	_
g - C_3N_4	2.00	2.03	2.13	2.34	2.32	2.33	_
	(4)	(4)	(4)	(4)	(2)	(2)	_
p-C ₃ N ₄	1.98	2.06	2.06	2.14	1.98	2.02	_
	(4)	(4)	(2)	(2)	(1)	(1)	_
C_3N_5	2.02	2.05	2.08	2.07	2.14	2.10	_
	(4)	(4)	(4)	(4)	(4)	(4)	_
S - N_2S	2.02	2.02	2.11	2.19	2.24	2.18	_
	(2)	(2)	(2)	(2)	(2)	(2)	_
T - N_2S	2.09	2.15	2.25	2.21	2.25	2.15	_
	(6)	(4)	(6)	(5)	(6)	(5)	_
$ \Delta q / e $							
C_9N_4	1.38	1.21	1.03	1.07	0.80	0.85	0.05
C_2N	1.32	0.97	0.95	0.99	0.71	0.75	0.07
BN	0.39	0.16	0.11	0.10	0.06	0.07	0.04
CTF	1.43	1.05	1.21	0.87	0.93	1.50	0.04
$C_2N_6S_3$	1.19	0.84	0.88	0.89	0.49	0.75	0.10
g - C_3N_4	0.86	0.60	0.59	0.45	0.28	0.20	0.07
p-C ₃ N ₄	0.70	0.42	0.19	0.14	0.09	0.12	0.08
C_3N_5	1.51	1.28	1.18	1.19	0.77	1.17	0.10
S - N_2S	0.99	0.97	0.94	0.86	0.46	0.50	0.16
T - N_2S	2.08	1.85	1.48	1.60	1.86	2.88	0.20

C₉N₄, C₂N₆S₃ and CTF, which indicates that the AM with the small adsorption energy of LPSs is "weak" to anchor the LPSs, while the AM with a medium adsorption energy of LPSs is "suitable" to hold the LPSs, in line with the Sabatier principle. 60

The migration barrier is also related to the diffusion constant

(D). 61 According to the formula: 62
$$D \sim \exp\left(\frac{E_{\rm a}}{k_{\rm B}T}\right)$$
, the diffusion

constant mainly depends on the value of the migration barrier without an external electric field, where E_a , k_B and T are the migration barrier, Boltzmann constant and temperature, respectively. Typically, the larger migration barrier prevents the diffusion of Li₂S₆ along Paths 1 and 3 on the C₉N₄ and C₂N₆S₃ monolayers. Moderate adsorption energies and migration energy barriers endow C₉N₄ and C₂N₆S₃ with a good adsorption effect on the LPSs, which is beneficial to inhibit the shuttle effect.

Table 2 Average length of Li-S bonds (d_{Li-S} , in Å) in free and adsorbed $\mathrm{Li_2S}_n$. Data in parentheses denote the number of Li-S bonds

	$\mathrm{Li}_2\mathrm{S}$	Li_2S_2	Li_2S_3	$\mathrm{Li}_2\mathrm{S}_4$	Li_2S_6	Li_2S_8
$\overline{\text{Li}_2S_n}$	2.09	2.23	2.33	2.38	2.40	2.38
	(2)	(4)	(4)	(4)	(4)	(4)
Li_2S_n (a) C_9N_4	2.39	2.47	2.51	2.51	2.47	2.69
	(2)	(4)	(3)	(3)	(3)	(4)
Li_2S_n @ C_2N	2.37	2.56	2.46	2.60	2.45	2.43
	(2)	(4)	(3)	(4)	(3)	(3)
Li_2S_n (a) BN	2.17	2.26	2.36	2.39	2.42	2.42
	(2)	(4)	(4)	(4)	(4)	(4)
Li_2S_n @CTF	2.53	2.46	2.52	2.69	2.62	2.63
	(2)	(3)	(3)	(3)	(4)	(3)
$\text{Li}_2S_n @ C_2N_6S_3$	2.69	2.45	2.50	2.49	2.49	2.46
	(2)	(4)	(3)	(4)	(4)	(4)
Li_2S_n ag- C_3N_4	2.23	2.40	2.42	2.53	2.41	2.50
0	(2)	(4)	(3)	(3)	(3)	(3)
Li_2S_n $p\text{-C}_3\text{N}_4$	2.27	2.49	2.40	2.44	2.45	2.43
	(2)	(4)	(4)	(4)	(4)	(4)
$\text{Li}_2\text{S}_n \otimes \text{C}_3\text{N}_5$	2.56	2.61	2.53	2.61	2.44	2.35
	(2)	(4)	(2)	(2)	(2)	(2)
$\text{Li}_2S_n \otimes S - \text{N}_2S$	2.74	2.51	2.51	2.50	2.48	2.41
	(2)	(4)	(4)	(4)	(4)	(4)
$\text{Li}_2S_n@T\text{-N}_2S$	2.77	2.44	2.58	2.58	2.57	2.77
2	(1)	(2)	(4)	(4)	(3)	(1)

Our above analyses indicate that the metallic C₉N₄ and C₂N₆S₃ monolayers are potential AM candidates for Li-S batteries.

3.3. Charge transfer analysis

To gain a deeper insight into the adsorption behavior of Li_2S_n on each AM, we examined the charge density difference and the charge transfer. The BN and CTF AMs were taken as the representatives again, and their charge distributions are displayed in Fig. 4, and the results for other systems are shown in Fig. S6 (ESI†). In general, for a given AM, as the adsorption energy decreases, the charge accumulation region between the Li2Sn and AM also decreases.

Table 1 summarizes the charge transfer (Δq) between the adsorbates and the AMs. Among all the considered ten AMs, T-N₂S has the largest amount of charge transfer with the adsorbed Li₂S_n, while the least charge transfer happens on BN. Upon adsorption, Li_2S_n loses electrons to the AM. In order to analyze the adsorption effect more intuitively, we checked the relationship between the absolute value of the charge transfer and the Li_2S_n adsorption energies as well as the Li-N bond lengths. As shown in Table 1, the greater charge transfer corresponds to a shorter Li–N bond length and a higher adsorption energy with the exception of T-N2S (the average bond length of the Li-N formed on T-N2S is the longest for Li_2S_n (n = 1, 2, 3, 6); however, the largest amount of charge transfer contributes to the largest number of Li-N bonds (Table 1) and S-N bonds (Table S4, ESI†)). For example, for the adsorption of Li_2S_n on C_9N_4 and C_2N , the same number of Li-N bonds is formed, while the average Li-N bond lengths (amount of charge transfer) on C₉N₄ are slightly shorter (larger) than for C2N. As a result, the adsorption energies are slightly larger on C₉N₄ than those on C₂N. To summarize, charge transfer analysis indicates that Δq is related to Li bonds, and corresponds to the adsorption strength. In addition to combining the charge density

PCCP Paper

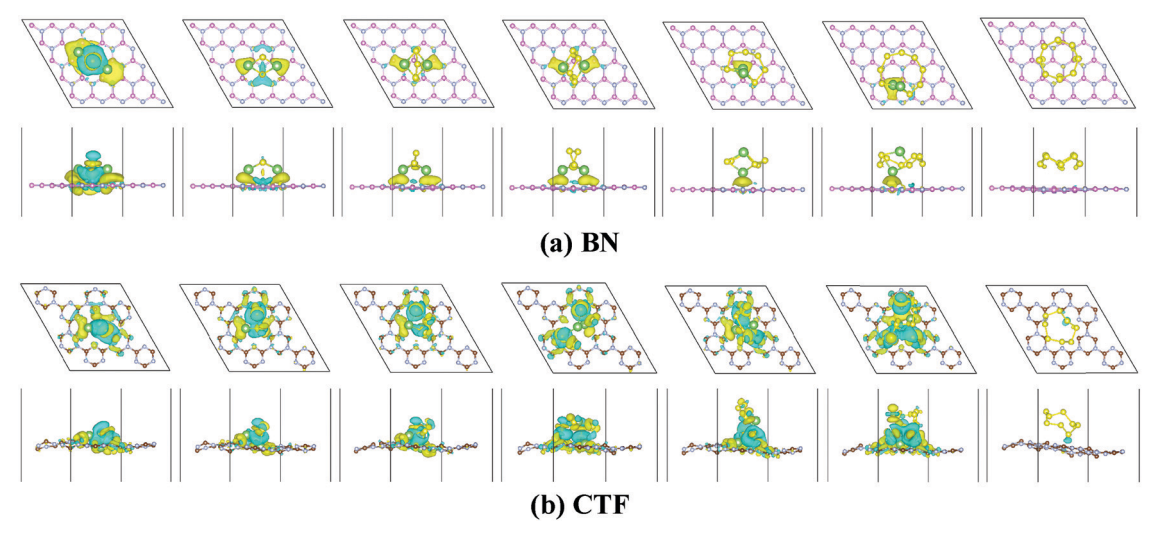


Fig. 4 Charge density difference diagrams of Li_2S_n and S_8 on BN (a) and CTF (b). The yellow and blue regions represent charge accumulation and depletion, respectively

difference diagrams (Fig. 4 and Fig. S6, ESI†) and the amount of charge transfer (Table 2) to judge the charge distribution of AMs-adsorbed Li_2S_n , the visualized planar average charge density difference can also be used to describe the charge transfer.⁶³

3.4. Effect of the N content and pore size on the Li bonds

Considering that the Li-N bonds correlate with the adsorption strength of the Li₂S_n clusters, and the Li-N bonds are formed at the pore region, we examined the effect of N content and pore size of the N-containing AMs on the Li-N bonds. Fig. 5 illustrates the variation of adsorption energy with the N content and pore size.

The relationship between the N-content and the adsorption energy of the LPSs on the AMs is a bit complicated. For C₉N₄, C₂N, C₂N₆S₃ and g-C₃N₄, they have the same number of bridge N atoms (m = 6) in one pore, and the E_{ad} value for the Li₂S_n species decreases as the N content increases (Fig. 5a). For g-C₃N₄

and p-C₃N₄ with equal N contents, the larger pore size of g-C₃N₄ allows the formation of more Li-N bonds, leading to the stronger adsorption strength. In general, the N content and number of bridge N atoms impacts on the adsorption strength.

Generally speaking, for a given Li_2S_n , the adsorption energy increases as the pore size increases (Fig. 5b), and the abrupt increase for T-N2S is due to the highest number of Li-N and S-N bonds being formed, since it has the largest N content (66.67%); the abnormal jump for CTF can be understood by the S-C bonds formed at the pore region; the deviation for C₂N₆S₃ is attributed to the lower charge transfer, which originates from the smaller electronegativity difference of S between C2N6S3 and the Li2Sn.

The effect of pore size on the Li bonds can also be understood by the adsorbed configurations of the Li_2S_n species. As shown in Fig. S1 (ESI†), in general, an AM with a larger pore size provides sufficient space to form more Li-N bonds, thus enhancing the adsorption strength and reducing the Li_2S_n shuttle effect.

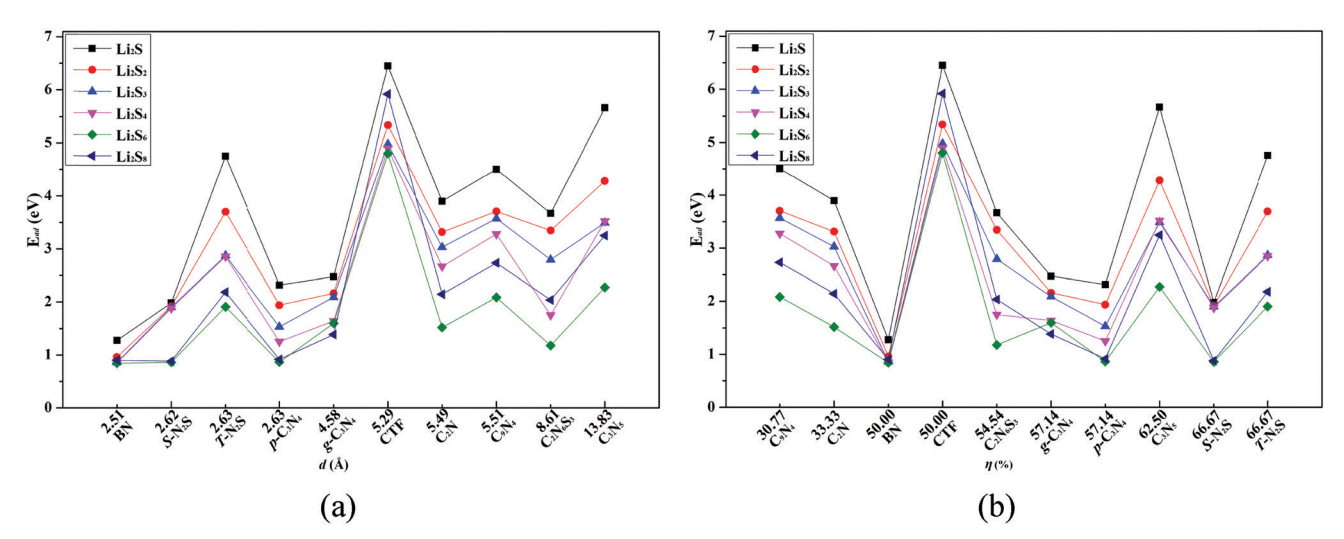
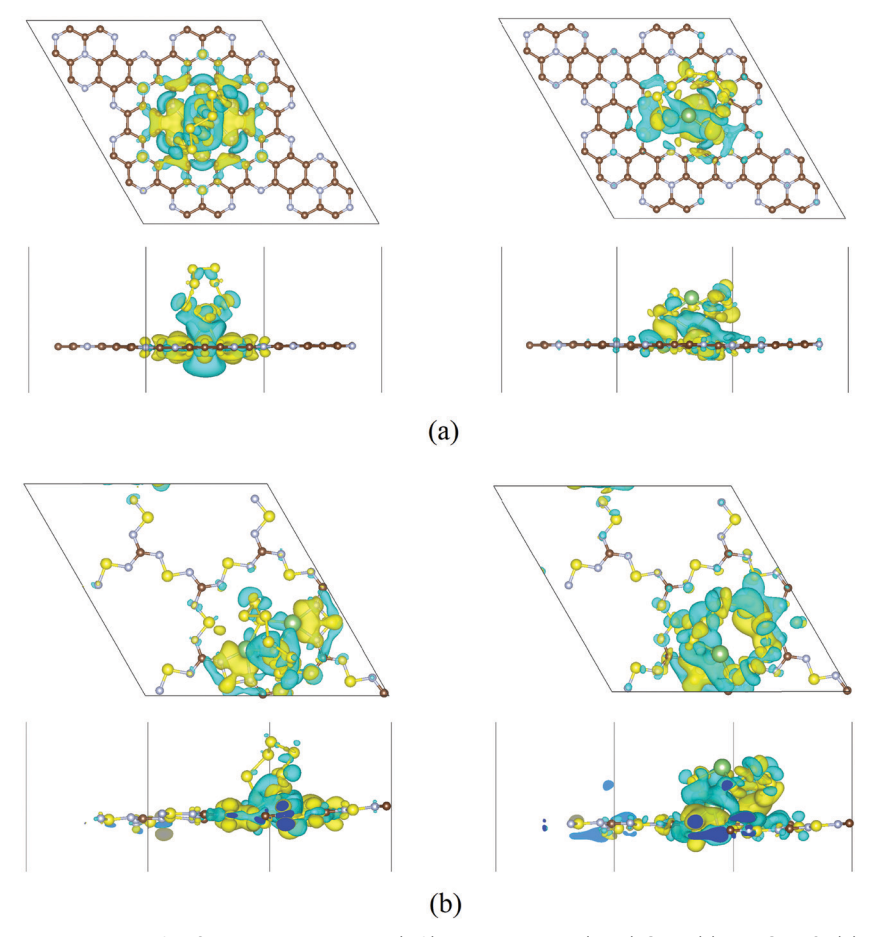


Fig. 5 Variation of the adsorption energy of Li_2S_n (n = 1-4, 6, 8) with the N content (a) and pore size (b) of the AMs. The diameters of the pore size and the values of the N contents are given in the x-axis for each AM.





Charge density difference diagram of Li_2S_8 on non-Li-trapped (left) and Li-trapped (right) C_9N_4 (a) and C_2N_6S_3 (b).

We found that there is a quasi-linear relationship between the adsorption energy and the pore size for eight out of the ten AMs examined in this work (except for CTF and T-N2S) (Fig. S7, ESI†). The slope decreases from Li₂S to the lowest value for Li₂S₆, and then increases slightly for Li₂S₈. This trend is consistent with the variation of adsorption energy as discussed in Section 3.1.

3.5. Adsorption of Li₂S₈ on Li-preadsorbed C₉N₄ and C₂N₆S₃

The adsorption of Li_2S_n on the AMs involves lots of complicated processes, e.g., Li-trapping in the AMs. 64,65 Thus, we investigated the effect of trapping one Li atom on the adsorption of the LPSs on the AMs. The C₉N₄ and C₂N₆S₃ monolayers were chosen as representative AMs due to their distinguished performance, and Li_2S_8 was selected as a delegate of the Li_2S_n since the long chain Li₂S₈ shows a dissociative tendency.

We compared the adsorption behavior of Li₂S₈ on non-/ Li-trapped C₉N₄ and C₂N₆S₃. Fig. 6 illustrates the energetically most favorable configuration and charge density difference diagram for Li₂S₈ on Li-trapped C₉N₄/C₂N₆S₃ and pristine C₉N₄/C₂N₆S₃ monolayers. For the case of Li-trapped C₉N₄/ C₂N₆S₃, charges are accumulated at the Li atom of the Li₂S₈ near C₉N₄/C₂N₆S₃, the two N atoms of the C₉N₄/C₂N₆S₃ monolayer, the S atom at the end of the S ring of Li₂S₈, and the precaptured Li atom. The adsorption energy and amount of charge transfer of Li₂S₈ on Li-trapped C₉N₄/C₂N₆S₃ are 1.87/1.46 eV and 0.08/0.17 | e | (Table S6, ESI†) respectively, which are lower than those on the pristine C_9N_4 monolayer ($E_{ad} = 2.73$ / 2.03 eV, $\Delta q = 0.85/0.75 |e|$). For Li-trapped $C_9N_4/C_2N_6S_3$, the charge of the Li atom precaptured by C₉N₄/C₂N₆S₃ compensates for the charge of the two S atoms at the end of the S ring in Li₂S₈, thus the total charge transfer amount of Li₂S₈ is reduced. The adsorption orientation of Li₂S₈ is "parallel" to Li-preadsorbed C₉N₄/C₂N₆S₃, compared with the "perpendicular" configuration in the pristine $C_9N_4/C_2N_6S_3$. Upon adsorption on the Li-trapped $C_9N_4/C_9N_6S_3$. C₂N₆S₃, the Li–S bond in the Li₂S₈ cluster is shortened from 2.69/ 2.46 to 2.44/2.35 Å without any dissociation tendency; the Li-N bonds nearly remain the same length (changing from 2.03/2.08 to 2.04/2.11 Å), while the number of Li-N bonds is reduced from 4/4 to 2/2. All these factors correspond to the decrease in adsorption energy. Therefore, it is very likely that the preadsorption of Li is beneficial for effective adsorption of Li_2S_n without dissociating long chain LPSs.

4. Conclusions

By means of comprehensive computations and comparison of the adsorption behavior of Li_2S_n (n = 1, 2, 3, 4, 6, 8) on ten N-containing monolayers (BN, C₂N, C₂N₆S₃, C₉N₄, CTF, g-C₃N₄,

p-C₃N₄, C₃N₅, S-N₂S and T-N₂S) as anchoring materials (AMs), we found that the Li bonds contribute to inhibiting the shuttle effect in Li-S batteries: the length and number of Li-N bonds are related to the pore size and N content of the 2D N-containing AMs, and correlate with the charge transfer between Li_2S_n and 2D AMs and the adsorption strength of LPSs on the 2D N-containing AMs. Among the ten considered AMs, the C₉N₄ and C₂N₆S₃ monolayers outperform the others as promising AMs for Li-S batteries, due to their metallic feature and "optimal" Li bonds: their moderate adsorption strength, and the "intact" configuration of the adsorbed LPSs, especially for the long chain clusters. Moreover, the porous framework and the high specific surface area of the C₉N₄ and C₂N₆S₃ monolayers will also provide fast ion transport and a broad reaction interface of the sulfur cathode, facilitating the high capacity output and superior rate performance of Li-S batteries. Thus, by taking advantage of Li bonds, we may reduce the notorious polysulfide shuttle effect, and facilitate the rational designing of 2D AMs for Li-S batteries.

Conflicts of interest

The authors declare no conflict of interest.

Acknowledgements

The authors gratefully acknowledge the financial support from the National Natural Science Foundation of China (11828401, 11964022) and Startup Project of Inner Mongolia University (21200-5175101), and in the USA by NSF Center for the Advancement of Wearable Technologies (Grant 1849243) and NASA (Grant Number 80NSSC19M0236).

References

- 1 X. L. Ji and L. F. Nazar, Advances in Li-S Batteries, *J. Mater. Chem.*, 2010, **20**, 9821–9826.
- 2 M. M. Thackeray, C. Wolverton and E. D. Isaacs, Electrical energy storage for transportation-approaching the limits of, and going beyond, lithium-ion batteries, *Energy Environ. Sci.*, 2012, 5, 7854–7863.
- 3 P. G. Bruce, L. J. Hardwick and K. M. Abraham, Lithium-air and lithium-sulfur batteries, *MRS Bull.*, 2011, **36**, 506–512.
- 4 C. Barchasz, F. Mesguich, J. Dijon, J. C. Lepretre, S. Patoux and F. Alloin, Novel positive electrode architecture for rechargeable lithium/sulfur batteries, *J. Power Sources*, 2012, **211**, 19–26.
- 5 L. F. Nazar, M. Cuisinier and Q. Pang, Lithium-sulfur batteries, MRS Bull., 2014, 39, 436–442.
- 6 A. Rosenman, E. Markevich, G. Salitra, D. Aurbach, A. Garsuch and F. Chesneau, Review on Li-sulfur battery systems: an integral perspective, *Adv. Energy Mater.*, 2015, 5, 1500212.
- 7 A. Manthiram, S. H. Chung and C. Zu, Lithium–sulfur batteries: progress and prospects, *Adv. Mater.*, 2015, **27**, 1980–2006.
- 8 Y. X. Yin, S. Xin, Y. G. Guo and L. J. Wan, Lithium–sulfur batteries: electrochemistry, materials, and prospects, *Angew. Chem., Int. Ed.*, 2013, **52**, 13186–13200.

- 9 Y. Yuan, G. Zheng and Y. Cui, Nanostructured sulfur cathodes, *Chem. Soc. Rev.*, 2013, 42, 3018–3032.
- 10 G. Zheng, Q. Zhang, J. J. Cha, Y. Yang, W. Li, Z. W. She and Y. Cui, Amphiphilic surface modification of hollow carbon nanofibers for improved cycle life of lithium sulfur batteries, *Nano Lett.*, 2013, 13, 1265–1270.
- 11 Q. Zhang, Y. Wang, Z. W. Seh, Z. Fu, R. Zhang and Y. Cui, Understanding the anchoring effect of two-dimensional layered materials for lithium–sulfur batteries, *Nano Lett.*, 2015, 15, 3780–3786.
- 12 T.-Z. Hou, H. J. Peng, J.-Q. Huang, Q. Zhang and B. Li, The formation of strong-coupling interactions between nitrogendoped graphene and sulfur/lithium (poly)sulfides in lithiumsulfur batteries, 2D Mater., 2015, 2, 014011.
- 13 T. Z. Hou, X. Chen, H. J. Peng, J. Q. Huang, B. Q. Li, Q. Zhang and B. Li, Design principles for heteroatom-doped nanocarbon to achieve strong anchoring of polysulfides for lithium–sulfur batteries, *Small*, 2016, **12**, 3283–3291.
- 14 F. Li, Y. Su and J. Zhao, Shuttle inhibition by chemical adsorption of lithium polysulfides in B and N co-doped graphene for Li-S batteries, *Phys. Chem. Chem. Phys.*, 2016, **18**, 25241–25248.
- 15 F. Li and J. Zhao, Atomic sulfur anchored on silicene, phosphorene, and borophene for excellent cycle performance of Li–S batteries, ACS Appl. Mater. Interfaces, 2017, 9, 42836–42844.
- 16 Y. Zhao, L. Yang, J. Zhao, Q. Cai and P. Jin, How to make inert boron nitride nanosheets active for the immobilization of polysulfides for lithium–sulfur batteries: a computational study, *Phys. Chem. Chem. Phys.*, 2017, 19, 18208–18216.
- 17 J. Wu and L. Wang, 2D framework C₂N as a potential cathode for lithium-sulfur batteries: an ab initio density functional study, *J. Mater. Chem. A*, 2018, **6**, 2984–2994.
- 18 K. Liao, P. Mao, N. Li, M. Han, J. Yi, P. He, Y. Sun and H. Zhou, Stabilization of polysulfides via lithium bonds for Li-S batteries, *J. Mater. Chem. A*, 2016, 4, 5406–5409.
- 19 Q. Pang and L. F. Nazar, Long-life and high areal capacity Li-S batteries enabled by a light-weight polar host with intrinsic polysulfide adsorption, ACS Nano, 2016, 10, 4111–4118.
- 20 J. Liang, L. Yin, X. Tang, H. Yang, W. Yan, L. Song, H. M. Cheng and F. Li, Kinetically enhanced electrochemical redox of polysulphides on polymeric carbon nitrides for improved lithium-sulphur batteries, ACS Appl. Mater. Interfaces, 2016, 8, 25193–25201.
- 21 C. Y. Fan, H. Y. Yuan, H. H. Li, H. F. Wang, W. L. Li, H. Z. Sun, X. L. Wu and J. P. Zhang, The effective design of a polysulfide-trapped separator at the molecular level for high energy density Li-S batteries, *ACS Appl. Mater. Interfaces*, 2016, **8**, 16108–16115.
- 22 Z. Meng, Y. Xie, T. Cai, Z. Sun, K. Jiang and W. Q. Han, Graphene-like *g*-C₃N₄ nanosheets/sulfur as cathode for lithium–sulfur battery, *Electrochim. Acta*, 2016, **210**, 829–836.
- 23 Z. Jia, H. Zhang, Y. Yu, Y. Chen, J. Yan, X. Li and H. Zhang, Trithiocyanuric acid derived g-C₃N₄ for anchoring the polysulfide in Li-S batteries application, *J. Energy Chem.*, 2020, 43, 71–77.

PCCP

24 K. Liao, X. Wang, Y. Sun, D. Tang, M. Han, P. He, X. Jiang, T. Zhang and H. Zhou, An oxygen cathode with stable full discharge-charge capability based on 2D conducting oxide, Energy Environ. Sci., 2015, 8, 1992-1997.

- 25 E. P. Kamphaus and P. B. Balbuena, Long-Chain Polysulfide Retention at the Cathode of Li-S Batteries, I. Phys. Chem. C, 2016, 120(8), 4296-4305.
- 26 D. N. Shigorin, Infra-red absorption spectra study of H-bonding and of metal-element bonding, Spectrochim. Acta, 1959, 14, 198-212.
- 27 A. B. Sannigrahi, T. Kar, B. G. Niyogi, P. Hobza and P. V. R. Schleyer, The lithium bond reexamined, Chem. Rev., 1990, 90, 1061-1076.
- 28 K. Park, J. H. Cho, J.-H. Jang, B.-C. Yu, A. T. De La Hoz, K. M. Miller, C. J. Ellisonab and J. B. Goodenough, Trapping lithium polysulfides of a Li-S battery by forming lithium bonds in a polymer matrix, Energy Environ. Sci., 2015, 8, 2389-2395.
- 29 T. Z. Hou, W. T. Xu, X. Chen, H. J. Peng, J. Q. Huang and O. Zhang, Lithium bond chemistry in lithium-sulfur batteries, Angew. Chem., Int. Ed., 2017, 56, 8178-8182.
- 30 X. Chen, Y.-K. Bai, C.-Z. Zhao, X. Shen and Q. Zhang, Lithium bond in lithium batteries, Angew. Chem., Int. Ed., 2020, 59, 11192-11195.
- 31 H. Chen, S. Zhang, W. Jiang, C. Zhang, H. Guo, Z. Liu, Z. Wang, F. Liu and X. Niu, Prediction of two-dimensional nodal-line semimetals in a carbon nitride covalent network, J. Mater. Chem. A, 2018, 6, 11252-11259.
- 32 J. Mahmood, E. K. Lee, M. Jung, D. Shin, I. Y. Jeon, S. M. Jung, H. J. Choi, J. M. Seo, S. Y. Bae, S. D. Sohn, N. Park, J. H. Oh, H. J. Shin and J. B. Baek, Nitrogenated holey twodimensional structures, Nat. Commun., 2015, 6, 6486.
- 33 Y. Zheng, H. Li, H. Yuan, H. Fan, W. Li and J. Zhang, Understanding the anchoring effect of Graphene, BN, C2N and C₃N₄ monolayers for lithium-polysulfides in Li-S batteries, Appl. Surf. Sci., 2018, 434, 596-603.
- 34 X. Jiang, P. Wang and J. Zhao, 2D covalent triazine framework: a new class of organic photocatalyst for water splitting, J. Mater. Chem. A, 2015, 3, 7750-7758.
- 35 L. Wei, X. Zhang, X. Liu, H. Zhou, B. Yang and M. Zhao, Tunable Dirac cones in two-dimensional covalent organic materials: C₂N₆S₃ and its analogs, RSC Adv., 2017, 7, 52065-52070.
- 36 D. M. Teter and R. J. Hemley, Low-compressibility carbon nitrides, Science, 1996, 271, 53-55.
- 37 M. Groenewolt and M. Antonietti, Synthesis of g-C₃N₄ nanoparticles in mesoporous silica host matrices, Adv. Mater., 2005, 17, 1789-1791.
- 38 Y. Zhang, T. Mori and J. Ye, Polymeric carbon nitrides semiconducting properties and emerging applications in photocatalysis and photoelectrochemical energy conversion, Sci. Adv. Mater., 2012, 4, 282-291.
- 39 H. Dong, A. R. Oganov, Q. Zhu and G. R. Qian, The phase diagram and hardness of carbon nitrides, Sci. Rep., 2014, 5, 9870.
- 40 P. Kumar, E. Vahidzadeh, U. K. Thakur, P. Kar, K. M. Alam, A. Goswami, N. Mahdi, K. Cui, G. M. Bernard, V. K. Michaelis

- and K. Shankar, C3N5: a low bandgap semiconductor containing an azo-linked carbon nitride framework for photocatalytic, photovoltaic and adsorbent applications, J. Am. Chem. Soc., 2019, 141, 5415-5436.
- 41 L. Huang, Z. Liu, W. Chen and D. Cao, and A. Zheng. Twodimensional graphitic C₃N₅ materials: promising metal-free catalysts and CO2 adsorbent, J. Mater. Chem. A, 2018, 6, 7168-7717.
- 42 F. Li, X. Lv, J. Gu, K. Tu, J. Gong, P. Jin and Z. Chen, Semiconducting SN₂ monolayer with three-dimensional auxetic properties: a global minimum with tetracoordinated sulfurs, Nanoscale, 2020, 12, 85-92.
- 43 J. H. Lin, H. Zhang, X. L. Cheng and Y. Miyamoto, Twodimensional wide-band-gap nitride semiconductors: singlelayer 1T-XN₂ (X = S, Se, and Te), Phys. Rev. B, 2016, 94, 195404.
- 44 S. S. Zhang, Liquid electrolyte lithium/sulfur battery: Fundamental chemistry, problems, and solutions, J. Power Sources, 2013, 231, 153-162.
- 45 G. Kresse and J. Hafner, Ab initio Hellmann-Feynman molecular dynamics for liquid metals, J. Non-Cryst. Solids, 1993, 156, 956-960.
- 46 G. Kresse and J. Hafner, Ab initio molecular-dynamics simulation of the liquid-metal-amorphous-semiconductor transition in germanium, Phys. Rev. B: Condens. Matter Mater. Phys., 1994, 49, 14251-14269.
- 47 G. Kresse and J. Furthmüller, Efficiency of ab-initio total energy calculations for metals and semiconductors using a plane-wave basis set, Comput. Mater. Sci., 1996, 6, 15-50.
- 48 G. Kresse and J. Furthmüller, Efficient iterative schemes for ab initio total-energy calculations using a plane-wave basis set, Phys. Rev. B: Condens. Matter Mater. Phys., 1996, 54, 11169-11186.
- 49 G. Kresse and D. Joubert, From ultrasoft pseudopotentials to the projector augmented-wave method, Phys. Rev. B: Condens. Matter Mater. Phys., 1999, 59, 1758-1775.
- 50 S. Baroni, P. Giannozzi and A. Testa, Green's-function approach to linear response in solids, Phys. Rev. Lett., 1987, 58, 1861-1864.
- 51 P. E. Blöchl, Projector augmented-wave method, Phys. Rev. B: Condens. Matter Mater. Phys., 1994, 50, 17953-17979.
- 52 J. P. Perdew, K. Burke and M. Ernzerhof, Generalized gradient approximation made simple, Phys. Rev. Lett., 1996, 77, 3865.
- 53 T. Li, C. He and W. Zhang, Two-dimensional porous transition metal organic framework materials with strongly anchoring ability as lithium-sulfur cathode, Energy Storage Mater., 2020, 25, 866-875.
- 54 T. Bucko, J. Hafner, S. Lebegue and J. G. Aangyan, Improved description of the structure of molecular and layered crystals: Ab Initio DFT calculations with van der Waals corrections, J. Phys. Chem. A, 2010, 114(43), 11814-11824.
- 55 R. F. W. Bader, A quantum theory of molecular structure and its applications, Chem. Rev., 1991, 91, 893-928.
- 56 G. Henkelman, A. Arnaldsson and H. Johnsson, A fast and robust algorithm for Bader decomposition of charge density, Comput. Mater. Sci., 2006, 36, 354-360.
- 57 E. Sanville, S. D. Kenny, R. Smith and G. Henkelman, Improved grid-based algorithm for Bader charge allocation, J. Comput. Chem., 2007, 28, 899-908.

Paper

- 58 G. Henkelman, B. P. Uberuaga and H. Jónsson, A climbing image nudged elastic band method for findingsaddle points and minimum energy paths, J. Chem. Phys., 2000, 113, 9901-9904.
- 59 J. Zhao, Y. Yang, R. S. Katiyard and Z. Chen, Phosphorene as a promising anchoring material forlithium-sulfur batteries: a computational study, J. Mater. Chem. A, 2016, 4, 6124-6130.
- 60 P. Sabatier, La Catalyse en Chimie Organique, Librairie Polytechnique, Paris et Liège, 1920.
- 61 T. Li, C. He and W. Zhang, Rational design of porous carbon allotropes as anchoring materials for lithium sulfur batteries, J. Energy Chem., 2021, 52, 121-129.
- 62 W. Li, Y. Yang, G. Zhang and Y. Zhang, Ultrafast and directional diffusion of Lithium in phosphorene for

- high-performance lithium-ion Battery, Nano Lett., 2015, 15, 1691-1697.
- 63 W. X. Zhang, Y. Yin and C. He, Lowering the Schottky barrier height of G/WSSe van der Waals heterostructures by changing theinterlayer coupling and applying external biaxial strain, Phys. Chem. Chem. Phys., 2020, 22, 26231-26240.
- 64 G. S. Yi, E. S. Sim and Y. Chung, Effect of lithium-trapping on nitrogen-doped graphene as an anchoring material for lithium-sulfur batteries: a density functional theory study, Phys. Chem. Chem. Phys., 2017, 19, 28189-28194.
- 65 C. Y. Liu and E. Y. Li, Adsorption mechanisms of lithium polysulfides on graphene-based interlayers in lithium sulfur batteries, ACS Appl. Energy Mater., 2018, 1, 455-463.